Dissociation Kinetics of Singly Protonated Leucine Enkephalin Investigated by Time-Resolved Photodissociation Tandem Mass Spectrometry

Jeong Hee Moon,[a] So Hee Yoon,[b] Yong Jin Bae,[b] and Myung Soo Kim[b]
[a] Medical Proteomics Research Center, KRIBB, Daejeon, Korea
[b] Department of Chemistry, Seoul National University, Seoul, Korea

The yields of post-source decay (PSD) and time-resolved photodissociation (PD) at 193 and 266 nm were measured for singly protonated leucine enkephalin ($[YGGFL + H]^+$), a benchmark in the study of peptide ion dissociation, by using tandem time-of-flight mass spectrometry. The peptide ion was generated by matrix-assisted laser desorption ionization (MALDI) using 2,5-dihydroxybenzoic acid as the matrix. The critical energy (E_0) and entropy ($\Delta S^‡$ at 1000 K) for the dissociation were determined by Rice-Ramsperger-Kassel-Marcus fit of the experimental data. MALDI was done for a mixture of YGGFL and Y_6 and the plume temperature determined by the kinetic analysis of $[Y_6 + H]^+$ data were used to improve the precision of E_0 and $\Delta S^‡$ for $[YGGFL + H]^+$. E_0 and $\Delta S^‡$ thus determined ($E_0 = 0.67 \pm 0.08$ eV, $\Delta S^‡ = -24.4 \pm 3.2$ eu with 1 eu = 4.184 J $K^{-1}mol^{-1}$) were significantly different from those determined by blackbody infrared radiative dissociation (BIRD) ($E_0 = 1.10$ eV, $\Delta S^‡ = -14.9$ eu), and by surface-induced dissociation (SID) ($E_0 = 1.13$ eV, $\Delta S^‡ = -10.3$ eu). Analysis of the present experimental data with the SID kinetics (and BIRD kinetics also) led to an unrealistic situation where not only PSD and PD but also MALDI-TOF signals could not be detected. As an explanation for the discrepancy, it was suggested that transition-state switching occurs from an energy bottleneck (SID/BIRD) to an entropy bottleneck (PSD/PD) as the internal energy increases. (J Am Soc Mass Spectrom 2010, 21, 1151–1158) © 2010 Published by Elsevier Inc. on behalf of American Society for Mass Spectrometry

Tandem mass spectrometry—detection of product ions from a mass-selected precursor ion—for peptide ions is widely used for protein sequencing [1, 2]. Importance of this method has led to active investigation of the dissociation mechanisms of peptide ions [3–5]. Attempts [6–8] have also been made to understand the details of the reaction paths leading to major product ions such as b- and y-type ions, which include the quantum chemical search [9–11] for the reaction paths. There are not many reports on the dissociation kinetics of peptide ions, even though the information available from such studies will be useful for detailed understanding of the process. Williams and coworkers reported kinetic and dynamic data for some peptide ions determined by blackbody infrared radiative dissociation (BIRD) [12–14]. Laskin and coworkers reported similar data obtained by analyzing time- and energy-resolved surface-induced dissociation (SID) [15, 16] yields.

Recently, we developed a time-resolved photodissociation (PD) method [17–21] to study dissociation kinetics of peptide ions generated by matrix-assisted laser desorption ionization (MALDI) using a tandem time-of-flight (TOF) mass spectrometer equipped with a reflectron analyzer. A peptide ion beam was irradiated by a UV laser (193 and 266 nm) pulse at the first time-focusing position of the instrument and product ions formed by PD were analyzed by the reflectron. To obtain time-resolved information, photoexcitation was done inside a cell floated at high voltage such that the product ions formed inside and outside the cell would be separated in the TOF spectrum. The technique allowed estimation of the photodissociation rate constant for a peptide ion [20]. We also observed evidence [18, 19] that the dissociation of peptide ions occurred in qualitative agreement with Rice-Ramsperger-Kassel-Marcus (RRKM) theory [22, 23]. To determine the dynamic parameters for dissociation, viz. critical energy (E_0) and entropy ($\Delta S^‡$), the theoretical yields of PD occurring inside and outside the cell and that of the spontaneous decay [post-source decay (PSD)] were calculated by RRKM and compared with experimental data. It is known [5, 6] that charge-directed cleavages of amide bonds are mainly responsible for the dissociation of peptide ions without an arginine residue(s), generating b- and y-type product ions. We estimated the total

Address reprint requests to Professor M. S. Kim, Department of Chemistry, Seoul National University, Seoul 151-742, Korea. E-mail: myungsoo@snu.ac.kr

1044-0305/10/$32.00
doi:10.1016/j.jasms.2010.03.025

Published online March 27, 2010
Received February 12, 2010
Revised March 12, 2010
Accepted March 17, 2010

rate constant for the dissociation of a peptide ion by assuming similar dissociation kinetics for different b/y channels. To narrow down the (E_0, $\Delta S^{\ddagger}$) sets compatible with experimental data, product ion yields measured for a peptide ion generated by MALDI with two or more matrices were utilized [19–21].

Singly protonated leucine enkephalin, [YGGFL + H]$^+$, is a benchmark peptide ion studied previously by BIRD [14] and SID [16]. Even though we wanted to determine E_0 and $\Delta S^{\ddagger}$ for this peptide ion by PD-tandem TOF and compare with the previous results, we experienced some difficulty because its dissociation occurred very fast at high internal energy. In this work, a method has been devised to improve the precision in their determination. E_0 and $\Delta S^{\ddagger}$ thus determined are similar to those for other peptide ions studied by PD-tandem TOF but significantly different from BIRD and SID results. A plausible explanation for such differences is also presented in this paper.

Experimental

A schematic drawing of the homebuilt MALDI-tandem TOF used in this work is shown in Figure 1. The original instrument [24] was modified recently to improve its performance [25]. A brief description of the instrument and its operation is as follows.

The instrument consists of a MALDI source with delayed extraction, a first stage TOF analyzer to time-separate the prompt ions generated by MALDI, an ion gate and a second stage TOF analyzer equipped with a reflectron, 337 nm pulse from a nitrogen laser is used for MALDI. Its intensity is kept at around 2.5× the threshold value. A cylindrically focused PD laser pulse at 266 or 193 nm passes through the first time focus in synchronization with the lowest *m/z* isotopomer of a peptide ion. The intensity of a PD laser is kept sufficiently low such that multiphoton absorption is not important. MCP detector output is treated as described previously [24], and averaged over 30,000 shots. Finally, the laser-off spectrum (PSD) is subtracted from the laser-on spectrum to obtain the laser-induced change or the PD spectrum. As in the original instrument [24], the potential inside the reflectron in the modified instrument [25] has both linear and quadratic components, $V = c_1x + c_2x^2$ with $c_1 = 15{,}317\ Vm^{-1}$ and $c_2 = 61{,}094\ Vm^{-2}$.

The PD cell installed for time-resolved study consists of four grid electrodes (E1-E4) as shown in Figure 1. E1 and E4 are grounded while E2 and E3 are floated at the same potential. Each product ion peak (m_2^+) in a voltage-off PD spectrum splits into several components when high voltage is applied to the cell—the one due to its formation from the precursor ion (m_1^+) inside (in-cell component, I) and outside (post-cell component, P) the cell, and the consecutive components ($m_1^+ \rightarrow m_i^+ \rightarrow m_2^+$, C) with the first step of the reaction ($m_1^+ \rightarrow m_i^+$) occurring inside the cell and the second step outside. I and C are due to dissociation of m_1^+ within around 0.07 μs after photoexcitation while P is due to dissociation occurring on the time scale of 0.1–4 μs.

From a PSD spectrum, we measure the Σ[product ion]/[precursor ion] ratio, which is called YPSD. From a voltage-on PD spectrum, we measure the sums of the intensities for all product ions formed outside (Σ[P]) and inside (Σ[I] + Σ[C]) the cell and take their ratio, Σ[P]/(Σ[I] + Σ[C]), which is called CPD. The method to calibrate the detector gain for each ion was reported previously [19].

Sample Preparation

The peptides used in this work, YGGFL and YYYYYY (= Y_6), the matrices, 2,5-dihydroxybenzoic acid (DHB) and α-cyano-4-hydroxycinnamic acid (CHCA), and other chemicals were purchased from Sigma (St. Louis, MO, USA). A matrix solution was prepared daily using acetonitrile and 0.1% trifluoroacetic acid and was mixed with a peptide solution containing YGGFL, Y_6, or 1:1 mixture of these. The final concentration of each peptide in the solutions prepared for PD experiments was 50 pmol/μL; 1 μL of the solution was loaded on the sample plate.

Computation

Previously [18, 19], we reported evidence that the dissociation of peptide ions proceed in qualitative accordance with the theory of mass spectra (RRKM-QET) [22, 23]. A method to calculate the RRKM rate-energy relation, $k(E)$, for a peptide ion was reported also [26, 27]. RRKM rate constant is virtually determined by two dynamic parameters, the critical energy (E_0) and entropy ($\Delta S^{\ddagger}$ at 1000 K). In addition to E_0 and $\Delta S^{\ddagger}$, the

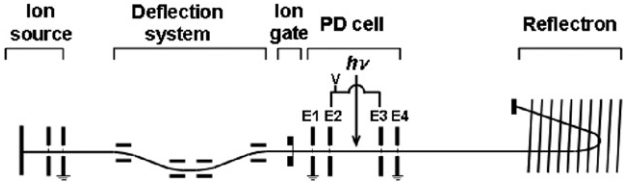

Figure 1. A schematic drawing of the homebuilt MALDI-tandem TOF used in this work. A deflection system consisting of four deflectors is installed in front of the ion gate to eliminate PSD product ions formed between the ion source and the ion gate. Details of the instrument and its operation are described in the Experimental section and in references [17–19, 25].

internal energy distribution for a peptide ion is needed to calculate its dissociation rate constant. For a peptide ion formed by MALDI, we proposed previously [19] to calculate it by assuming thermal equilibrium at an effective temperature (T).

Details of the method for RRKM fitting of the experimental data were reported previously [19]. The rate constant ($k(E)$) for the cleavage of an amide bond and the precursor ion internal energy distribution ($P_0(E)$) were calculated at specified E_0, $\Delta S^{\ddagger}$, and T. Cleavages of different amide bonds were assumed to be dynamically similar. Then, to mimic competition of these reactions, the total rate constant ($k_{tot}(E)$) was estimated by multiplying $k(E)$ by the number of amide bonds. Assuming the first-order kinetics for the decay of the precursor ion at each energy, $P_0(E) \times \exp[-k_{tot}(E)t]$, its survival probabilities at several important locations inside the apparatus were calculated. From these, the theoretical maximum and minimum values for YPSD were evaluated. The method to evaluate theoretical CPD was similar, except that the internal energy distribution function for the surviving precursor ions at the position of photoexcitation was shifted along the energy axis by $h\nu$. Then, when the experimental YPSD and CPD agreed with their theoretical counterparts within the maximum allowed error limits, the (E_0, $\Delta S^{\ddagger}$, T) set was taken. Otherwise, it was discarded. The selection process can be carried out using CPD and YPSD data simultaneously or one after another. In this work, the results from stepwise selection, first with CPD then with YPSD, will be shown for clarity. Calculations of YPSD and CPD and selection were done for many sets of (E_0, $\Delta S^{\ddagger}$, T)—nearly one hundred million.

Results

In peptide MALDI, it is generally thought that DHB is a colder matrix than CHCA [28], i.e., generates ions with lower internal energy, even though the opposite was reported in the matrix-assisted laser desorption of preformed ions [29]. DHB-MALDI was the most useful in our previous kinetic studies of peptide ion dissociation. Even though CHCA-MALDI was less useful, the results, when combined with the results from DHB-MALDI, helped to further narrow down the ranges of E_0 and $\Delta S^{\ddagger}$ [19–21]. Observations of smaller YPSD and larger CPD (smaller PD rate constant) with DHB than with CHCA and lower T determined by their kinetic analysis agree with the general consensus mentioned above.

PSD spectrum for [YGGFL + H]$^+$ formed by DHB-MALDI is shown in Figure 2a. [YGGFL + H]$^+$ generated by MALDI of the 1:1 mixture of YGGFL and Y_6 was selected by the ion gate to record this spectrum. The pattern of the spectrum measured from the YGGFL-only sample was very similar. YPSD of the two spectra could be made virtually identical by slight adjustment of the MALDI laser power. PSD spectrum recorded using CHCA as matrix (not shown) was also similar except that YPSD was larger. As was pointed out in a previous work, larger YPSD with CHCA is consistent with RRKM. YPSD measured with DHB-MALDI is listed in Table 1. PSD spectrum in Figure 2a is dominated by b_n, y_n, and their consecutive dissociation products. It is also similar to the spectra obtained by metastable ion decomposition (MID) [30] and collisionally activated dissociation (CAD) [4, 30]. However, its spectral pattern is a little different from those obtained by BIRD [14] and SID [16]. For example, y_n (n = 2–4) ions in BIRD and SID spectra are not as prominent as in PSD, MID, and CAD spectra. Such a difference may arise from the fact that slower dissociations of lower energy ions are probed in BIRD and SID than in PSD, MID, and CAD (electrospray ionization was used in BIRD and SID versus MALDI in PSD and fast atom bombardment in MID and CAD).

266 nm PD spectrum for [YGGFL + H]$^+$ formed by DHB-MALDI is shown in Figure 2b. Product ions appearing in this spectrum are similar to those in PSD except that ions at high m/z are either missing or very weak, probably due to their further dissociation. Each product ion peak in this spectrum splits into I, P, and C components when high voltage is applied to the cell, as shown in insets in this figure. One hundred ninety-three nm PD spectrum for [YGGFL + H]$^+$, shown in Figure 2c, looks similar to that at 266 nm. It is to be noted, however, that their voltage-on splitting patterns are somewhat different, i.e., as photon energy increases, P components get weaker in agreement with RRKM. As in our previous works [19–21], we hoped to narrow down the ranges of E_0 and $\Delta S^{\ddagger}$ by utilizing the results from CHCA-MALDI. However, the effort turned out to be futile because the dissociation at 193 nm occurred very fast, such that CPD was difficult to measure. CPDs measured with DHB-MALDI are listed in Table 1, together with the average PD rate constants estimated from them by using the first-order kinetics [20].

(E_0, $\Delta S^{\ddagger}$) sets determined by CPD data at 193 and 266 nm with DHB-MALDI are shown as the region surrounded by a closed curve in Figure 3 (E_0 in eV and $\Delta S^{\ddagger}$ in eu with 1 eu = 4.184 J K^{-1}mol^{-1}). It is to be mentioned that each point in this region represents different T. Inclusion of the YPSD analysis further limits (E_0, $\Delta S^{\ddagger}$) to the gray region. (E_0, $\Delta S^{\ddagger}$) sets for [YGGFL + H]$^+$ are more widely scattered than in our previous works [20, 21] that utilized both the results from DHB- and CHCA-MALDI data. E_0, $\Delta S^{\ddagger}$, and T averaged over the gray region are listed in Table 2. The errors quoted in the table were estimated at the 95% confidence limit ($\pm 1.96\sigma$).

The experimental data are compatible with a wide range of (E_0, $\Delta S^{\ddagger}$, T) sets because the influences of these parameters are interrelated. For example, decrease of $k(E)$ due to increase of E_0 can be more or less compensated by increase of T. If one of the three parameters is known, the ranges for the other two compatible with the experimental data will be narrowed. E_0 and $\Delta S^{\ddagger}$ are the dynamic parameters that we would like to deter-

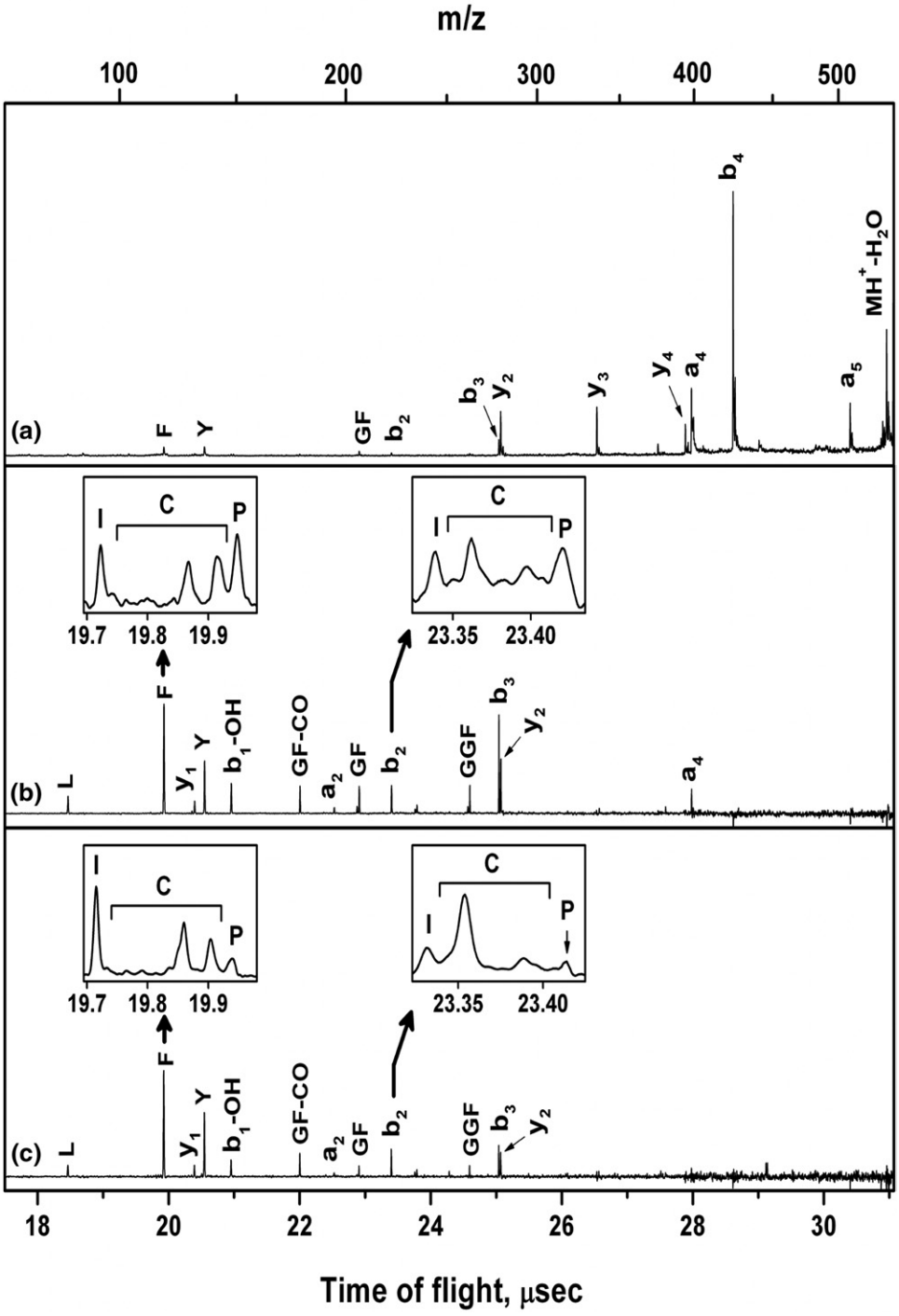

Figure 2. (**a**) PSD and PD spectra at (**b**) 266 nm and (**c**) 193 nm for $[YGGFL + H]^+$ formed by DHB-MALDI. In-cell (I), post-cell (P), and consecutive (C) components are marked in the 3 kV-on splitting patterns of b_2 and F product ions shown in insets of (**b**) and (**c**).

mine in this work. Hence, it will be desirable to have an independent estimate of T.

$[Y_6 + H]^+$ was a prototype system used in our previous study [19] on the dissociation dynamics of peptide ions without a basic residue. In a previous work [25], we determined E_0 and $\Delta S^{\ddagger}$ for its dissociation by three independently optimized, operated, and calibrated PD-tandem TOF instruments with somewhat different ion-optical characteristics. The results were essentially the same, indicating that the experimental factors that might affect the ion yield data had been well taken care of. Neither Y_6 nor YGGFL contains an acidic or basic amino acid residue, a factor that may affect T of a protonated peptide generated by MALDI. Hence, it may be reasonable to assume that the effective temperatures of $[Y_6 + H]^+$ and $[YGGFL + H]^+$ in the same

Table 1. YPSD and CPD data for $[YGGFL + H]^+$ formed by DHB-MALDI and average PD rate constants (in 10^7 s^{-1}) estimated from CPDs

	193 nm PD		266 nm PD	
YPSD	CPD	Average *k*	CPD	Average *k*
0.105	0.121	2.05	0.609	1.01

MALDI plume, i.e., the MALDI plume formed from the peptide mixture, are similar. Accordingly, we measured YPSD and CPD data for these peptide ions formed by MALDI of the peptide mixture, analyzed the data for $[Y_6 + H]^+$, and used the temperature range thus determined for the analysis of $[YGGFL + H]^+$ data. We would like to add that similar acid-base characteristics of $[Y_6 + H]^+$ and $[YGGFL + H]^+$ also lead us to expect similar E_0 and $\Delta S^‡$ for the charge-directed dissociation of these two peptide ions.

PSD and PD spectra for $[Y_6 + H]^+$ generated by DHB- and CHCA-MALDI were reported previously [19] and hence will not be shown. We will just mention that the PSD spectral patterns and YPSD obtained in this work became essentially the same as those obtained for Y_6-only sample when MALDI laser intensity was slightly adjusted. Then, CPD values were also reproducible. (E_0, $\Delta S^‡$) sets for $[Y_6 + H]^+$ determined by CPD data at 266 and 193 nm obtained with DHB-MALDI are shown as the region surrounded by a closed curve in Figure 4. Inclusion of the YPSD analysis further limits (E_0, $\Delta S^‡$) to the gray region. We determined another gray region by using data obtained with CHCA-MALDI and took the intersection of the two gray regions. The results are shown as the dark region in Figure 4. E_0, $\Delta S^‡$, and T averaged over the dark region are listed in Table 2. It is to be mentioned that E_0, $\Delta S^‡$, and T values for $[Y_6 + H]^+$ determined in this work are essentially the same as the corresponding values reported previously [20, 25]. At the 95% confidence limit, the effective temperature of $[Y_6 + H]^+$ lies in the range 366-486 K. We assumed the same range of T for $[YGGFL + H]^+$ and selected the (E_0, $\Delta S^‡$, T) sets from the gray region in Figure 3. The results are shown as the slashed region in the same figure. E_0, $\Delta S^‡$, and T averaged over this region are listed in Table 2. It is to be noted that E_0 and $\Delta S^‡$ for $[YGGFL + H]^+$ thus obtained are quite similar to the corresponding values for $[Y_6 + H]^+$, in agreement with our expectation. The average effective temperatures for the two peptide ions are a little different, even though well within the error limits.

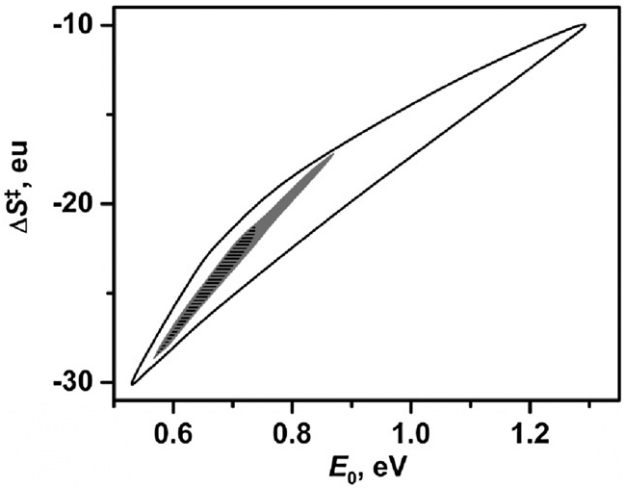

Figure 3. (E_0, $\Delta S^‡$) sets for the dissociation of $[YGGFL + H]^+$ formed by DHB-MALDI. The region surrounded by an outer closed curve was determined by using only CPD data at 193 and 266 nm. YPSD analysis limits the sets to the gray region. Assumption of the same effective temperature for $[YGGFL + H]^+$ and $[Y_6 + H]^+$ in the same MALDI plume further limits the sets to the slashed region.

Table 2. E_0 and $\Delta S^‡$ for $[YGGFL + H]^+$ and $[Y_6 + H]^+$ determined by PD, BIRD, and SID and the effective temperature (T) of the peptide ions formed by DHB-MALDI

	E_0, eV	$\Delta S^‡$, eu[a]	T, K	
$[YGGFL + H]^+$	0.71 ± 0.13	−22.9 ± 4.9	478 ± 77	PD[b]
	0.67 ± 0.08	−24.4 ± 3.2	454 ± 47	PD[c]
	1.10	−14.9		BIRD
	1.13	−10.3		SID
$[Y_6 + H]^+$	0.64 ± 0.10	−26.1 ± 6.0	426 ± 60	PD

[a]1 eu = 4.184 J $K^{-1}mol^{-1}$.
[b]DHB-MALDI results. The gray region in Figure 3.
[c]DHB-MALDI results with T from $[Y_6 + H]^+$. The slashed region in Figure 3.

$k_{tot}(E)$ for $[YGGFL + H]^+$ calculated with E_0 = 0.67 eV and $\Delta S^‡$ = −24.4 eu determined in this work is shown in Figure 5. The initial internal energy distribution, $P_0(E)$, for the same ion at T = 454 K also determined in this work is shown in Figure 6. We mentioned in the computational section that the energy distribution at any time t after ion formation was calculated by the first-order kinetics, $P_t(E) = P_0(E) \times \exp(-k_{tot}(E)t)$. The area under $P_t(E)$ corresponds to the relative inten-

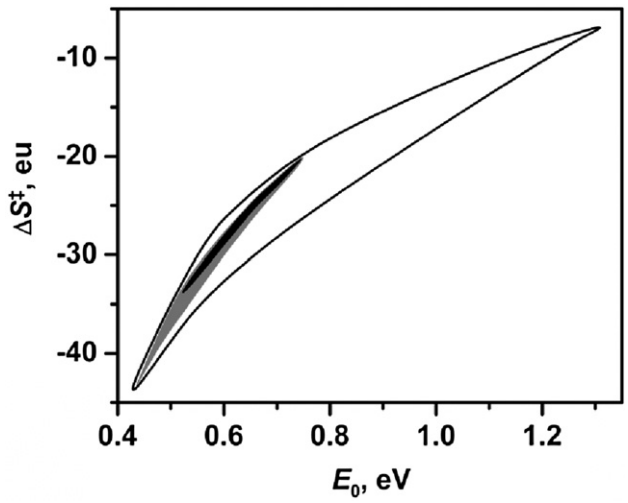

Figure 4. (E_0, $\Delta S^‡$) sets for the dissociation of $[Y_6 + H]^+$. Outer closed curve: use of CPD data only, DHB-MALDI. Gray region: CPD + YPSD, DHB-MALDI. Dark region: intersection of two gray regions from DHB- and CHCA-MALDI.

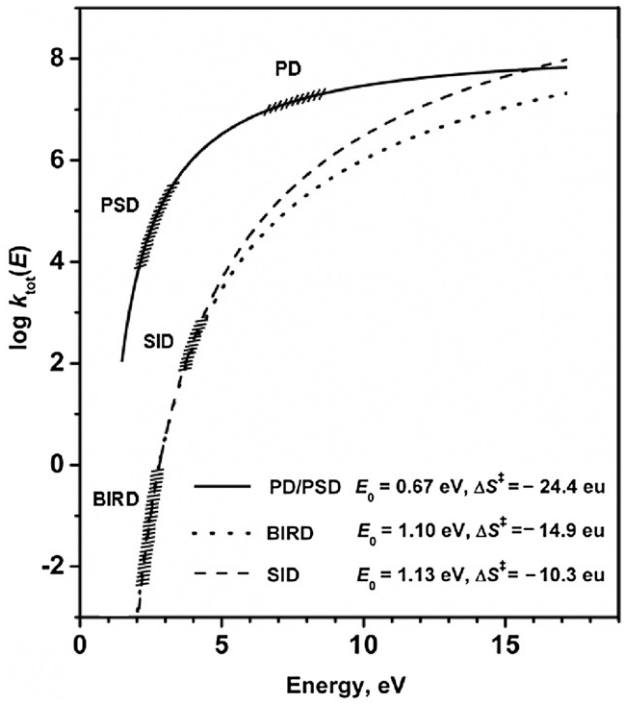

Figure 5. $k_{tot}(E)$ curves for $[YGGFL + H]^+$ calculated with E_0 and $\Delta S^{\ddagger}$ determined by PD/PSD (——), BIRD (· · · · · ·), and SID (----). The estimated rate constant range covered in each experiment is marked.

sity of the precursor ion at time t. The energy distribution for the precursor ion at the center of the PD cell, $P_2(E)$ (a notation used in reference [19]), is shown in Figure 6. The average internal energy calculated from $P_2(E)$ is 2.09 eV. Shifting $P_2(E)$ along the x-axis by photon energy results in the energy distribution for the photo-excited ion at the same position, $P_0(E)^{V*}$. $P_0(E)^{V*}$ curves upon 193 and 266 nm excitation are also shown in Figure 6. The average internal energies after 193 nm (6.42 eV) and 266 nm (4.66 eV) excitations are 8.51 and 6.75 eV, respectively. The average PD rate constants at 193 and 266 nm read from $k_{tot}(E)$ in Figure 5 at E = 8.51 and 6.75 eV are 2.02×10^7 and 1.03×10^7 s^{-1}, respectively, in agreement with the experimental values of 2.05×10^7 and 1.01×10^7 s^{-1}. This demonstrates that E_0, $\Delta S^{\ddagger}$, and T determined in this work are compatible with the experimental results.

Discussion

By the master equation modeling of BIRD data, Williams et al. [14] suggested that the dissociation of $[YGGFL + H]^+$ occurred in the 'rapid energy-exchange (REX)' limit with E_0 = 1.1 eV and the A factor of $10^{10.5}$ s^{-1}. The A factor in the REX limit, or A^{∞}, can be converted to $\Delta S^{\ddagger}$ at 1000 K by using a well known relation [31]. E_0 and $\Delta S^{\ddagger}$ thus estimated are listed in Table 2. Laskin [16] measured the time evolution of $[YGGFL + H]^+$ and its product ion signals in SID. E_0 and $\Delta S^{\ddagger}$ for the formation of seven product ions were determined via RRKM fit. E_0 = 1.13 eV was reported to be consistent with $k_{tot}(E)$ determined by combining individual decay rates. A $k_{tot}(E)$ of 5×10^5 s^{-1} at 8 eV from the kinetic modeling was quoted. The above data have been used in this work to estimate $\Delta S^{\ddagger}$ via RRKM calculation. $\Delta S^{\ddagger}$ thus estimated and E_0 are listed in Table 2. It is to be noted that E_0 and $\Delta S^{\ddagger}$ determined by BIRD and SID data are somewhat similar. On the other hand, they are significantly different from the present results.

$k_{tot}(E)$ curves calculated with E_0 and $\Delta S^{\ddagger}$ derived from SID and BIRD results, to be called $k_{tot}(E)_{SID}$ and $k_{tot}(E)_{BIRD}$, respectively, are shown in Figure 5. $k_{tot}(E)_{SID}$ is closer to the present curve than $k_{tot}(E)_{BIRD}$ is. We will see if $k_{tot}(E)_{SID}$ can explain our experimental observations. It is to be emphasized that the average PD rate constants measured in this work, such as 1.01×10^7 s^{-1} at 266 nm, are purely experimental results free from any assumption made in the kinetic analysis. The average internal energy corresponding to each rate constant can be determined once $k_{tot}(E)$ is known. Using $k_{tot}(E)_{SID}$, this is 11.85 eV after the photoexcitation at 266 nm. Then, the average internal energy at the center of the PD cell before photo-excitation becomes 7.19 eV. By calculating $P_2(E)$ as before, but using $k_{tot}(E)_{SID}$, we can estimate T resulting in this average internal energy at this position predicted by SID kinetics; 1090 K thus obtained seems to be higher than expected for DHB-MALDI—DHB is one of the coldest matrices in peptide MALDI [28]. Now, let us use $k_{tot}(E)_{SID}$ and investigate the dissociation of $[YGGFL + H]^+$ at 1090 K. In the apparatus used, a deflection system is installed in the region between the ion source and the first time focus to eliminate PSD product ions formed in this region. We calculated the energy distribution at the end of the deflection system using $k_{tot}(E)_{SID}$. The relative intensity of the precursor ion, or the area under this distribution, was 3.1×10^{-3}, i.e., only a tiny fraction of the precursor ions survived at the end of the deflection system. The

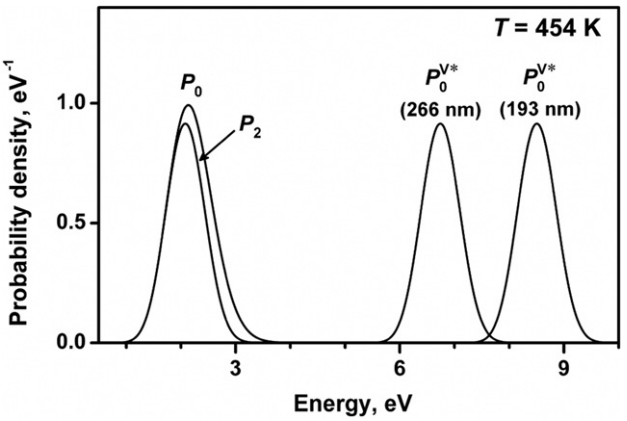

Figure 6. The initial internal energy distribution of $[YGGFL + H]^+$ formed by DHB-MALDI ($P_0(E)$, calculated at T = 454 K), the distribution at the center of the PD cell ($P_2(E)$), and the distributions after photoexcitation at 193 and 266 nm ($P_0(E)^{V*}$).

survival fraction at the detector, in the absence of photo-excitation, was 1.5×10^{-4}. The analysis made so far can be summarized as follows. We observed PSD and PD signals formed on the time scales of 10 μs and 100 ns, respectively. The attempt to analyze the observations using $k_{tot}(E)_{SID}$ ($k_{tot}(E)_{BIRD}$ also) resulted in an unrealistic situation that not only PSD and PD but also ordinary MALDI-TOF signals could not be easily detected. That is, the SID and BIRD kinetics are incompatible with our observation of PSD and PD signals on the time scales of 10 μs and 100 ns, respectively.

In this work, E_0 and $\Delta S^{\ddagger}$ were determined by a rather straightforward RRKM fitting of experimental data. Experimentally, we took care to control the factors that might affect the ion yield data such as the PD laser power. Also, based on the previous study [25] on $[Y_6 + H]^+$ using three instruments with different ion-optical layouts, we are confident that the instrumental factors such as mass discrimination are well taken care of. For reactions occurring via loose transition-state, it is known [32, 33] that RRKM fitting of experimental data tends to result in dissociation energies that are a little smaller (by 6% or less) than correct values. Such errors might be unimportant for the present reactions occurring via tight transition states. Even though the validity of RRKM fitting might be debatable, it is unlikely to be responsible for the differences mentioned above because the same assumption was also adopted in BIRD and SID works. In this work, $k_{tot}(E)$ was estimated by multiplying $k(E)$ for a typical bond by 4. To estimate the errors involved, we changed $k_{tot}(E)$ by a factor of 2, repeated the kinetic analysis, and found only $\pm$5% variation in the final results. Similar variation was observed when the error window for CPD was expanded from $\pm$30% in the original treatment to +100/−50%. One of the potential weaknesses in our approach is the assumption of thermal equilibrium for peptide ions formed by MALDI, even though the same assumption was made by other investigators [34, 35]. One can not rule out the possibility that some hyper-thermal peptide ions are formed in MALDI through photochemical reactions. Referring to our $k_{tot}(E)$ curve in Figure 5 and $P(E)$ in Figure 6, such ions would have dissociated almost completely by the time they arrive at the measurement region—a peptide ion exits the deflection system 7.8 μs after its formation. That is, with hyper-thermal peptide ions eliminated by PSD occurring between the ion source and the first time focus, the internal energy distribution for surviving ions might look near-thermal more than it might have been at the time of MALDI. The potential errors mentioned above may increase the inaccuracy in our results beyond the error limits quoted in this work. Regardless of the validity of the assumptions and related errors, however, the fact remains that the SID and BIRD kinetics are incompatible with our observation of PSD and PD signals on the time scales of 10 μs and 100 ns, respectively.

Significant difference between the results from PSD/PD and those from BIRD/SID is puzzling. In this regard, it is to be noted that BIRD and SID are observing ion dissociation on longer time scales than PSD and PD, 1–100 s for BIRD and 0.001–1 s for SID, which might be responsible for the observed difference. In the quantum chemical search for reaction path, Paizs and Suhai [9] and Siu et al. [11] found that many isomerization and tautomerization steps, with each step having its own barrier, were involved in the formation of b and y product ions. Let us suppose that two rate-affecting transition structures (TS) are present along a b/y reaction path, TS1 with large E_0 and large $\Delta S^{\ddagger}$ (energy bottleneck) and TS2 with small E_0 and small $\Delta S^{\ddagger}$ (entropy bottleneck). Then, the rate-determining TS can change from TS1 (SID/BIRD) to TS2 (PSD/PD) as the internal energy increases, a classic case of TS switching [36]. For PD and SID results to be reconciled, such a switching must occur at a smaller rate constant than observed in PD, i.e., 10^7 s^{-1}. $k_{tot}(E)$ curves calculated with PD and SID parameters cross indeed, but at $k_{tot} = 6 \times 10^7$ s^{-1}. To get TSS at a lower k_{tot}, either $k_{tot}(E)_{SID}$ and $k_{tot}(E)_{BIRD}$ must be shifted toward lower energy or $k_{tot}(E)_{PD}$ must be shifted toward higher energy, as can be seen from Figure 5.

In the quantum chemically found b/y reaction path for the dissociation of small model peptide ions [9, 11], the ionizing proton completely moves to an amide nitrogen and a five-membered ring involving this nitrogen is formed in TS. In our previous studies [19–21], both E_0 and $\Delta S^{\ddagger}$ were found to be significantly smaller than quantum chemical results (E_0 = 1.14 eV and $\Delta S^{\ddagger}$ = −0.86 eu for $[G_3 + H]^+$) [calculated at the geometries of the global minimum and the transition structure reported in reference 9] and decrease further in the presence of a basic residue, viz. lysine and histidine. Presence of intramolecular interaction in TS was suggested as an explanation for the highly negative $\Delta S^{\ddagger}$. Specifically, in addition to the five-membered ring in the original quantum chemical TS, another ring was suggested to form due to the interaction of the ionizing proton both with the reaction center and with a basic group, either the amino group at the N-terminus or a nitrogen atom in a basic residue. E_0 values for $[YGGFL + H]^+$ determined by SID and BIRD were similar to the above quantum chemical result and hence might be taken as evidence against the validity of our method and results. However, we have found in this work that E_0 and $\Delta S^{\ddagger}$ for $[YGGFL + H]^+$ determined by PD-tandem TOF are similar to those for $[Y_6 + H]^+$ and that SID and BIRD kinetics are incompatible with our observations. These suggest that an entropy bottleneck due to intramolecular interaction is rate-determining for rapid dissociation (PSD/PD) of a peptide ion, even if a higher energy barrier (energy bottleneck) might be present on the reaction path and limit the rate at low-energy (SID/BIRD). A more accurate rate-energy relation is needed to check whether TS switching between energy and entropy bottlenecks is indeed responsible for the

discrepancy between SID/BIRD and PSD/PD results. As part of such an effort, we are trying to devise a method to study PD over a wider energy range than in this work.

Acknowledgments

M.S.K. thanks Professor F. W. McLafferty for helpful discussion. The authors acknowledge financial support for this work by the National Research Foundation, Republic of Korea, and by the Bio-Signal Analysis Technology Innovation Program (M10645010002-06N4501-00,210) of the Ministry of Education, Science, and Technology (MEST), Republic of Korea. S.H.Y. and Y.J.B. thank MEST for Brain Korea 21 Fellowship.

References

1. Kinter, M.; Sherman, N. E. Protein Sequencing and Identification Using Tandem Mass Spectrometry; John Wiley: New York, 2000; p. 64–116, 238–268.
2. Hernandez, P.; Müller, M.; Appel, R. D. Automated Protein Identification by Tandem Mass Spectrometry: Issues and Strategies. *Mass Spectrom. Rev.* **2006,** *25,* 235–254.
3. Biemann, K. Sequencing of Peptides by Tandem Mass Spectrometry and High-Energy Collision-Induced Dissociation. In *Methods in Enzymology, Mass Spectrometry*, Vol. CXCIII; McCloskey, J. A., Ed.; Academic Press: New York, 1990; p. 455–479.
4. Ballard, K. D.; Gaskell, S. J. Sequential Mass Spectrometry Applied to the Study of the Formation of "Internal" Fragment Ions of Protonated Peptides. *Int. J. Mass Spectrom. Ion Processes* **1991,** *111,* 173–189.
5. Paizs, B.; Suhai, S. Fragmentation Pathways of Protonated Peptides. *Mass Spectrom. Rev.* **2005,** *24,* 508–548.
6. Wysocki, V. H.; Tsaprailis, G.; Smith, L. L.; Breci, L. A. Mobile and Localized Protons: A Framework for Understanding Peptide Dissociation. *J. Mass Spectrom.* **2000,** *35,* 1399–1406.
7. Polce, M. J.; Ren, D.; Wesdemiotis, C. Dissociation of the Peptide Bond in Protonated Peptides. *J. Mass Spectrom.* **2000,** *35,* 1391–1398.
8. Nold, M. J.; Wesdemiotis, C.; Yalcin, T.; Harrison, A. G. Amide Bond Dissociation in Protonated Peptides. Structures of the N-Terminal Ionic and Neutral Fragments. *Int. J. Mass Spectrom. Ion Processes* **1997,** *164,* 137–153.
9. Paizs, B.; Suhai, S. Combined Quantum Chemical and RRKM Modeling of the Main Fragmentation Pathways of Protonated GGG. II. Formation b_2, y_1, and y_2 Ions. *Rapid Commun. Mass Spectrom.* **2002,** *16,* 375–389.
10. Paizs, B.; Suhai, S. Towards Understanding the Tandem Mass Spectra of Protonated Oligopeptides. 1: Mechanism of Amide Bond Cleavage. *J. Am. Soc. Mass Spectrom.* **2004,** *15,* 103–113.
11. Aribi, H. E.; Rodriquez, C. F.; Almeida, D. R. P.; Ling, Y.; Mak, W. W.-N.; Hopkinson, A. C.; Siu, K. W. M. Elucidation of Fragmentation Mechanisms of Protonated Peptide Ions and Their Products: A Case Study on Glycylglycylglycine Using Density Functional Theory and Threshold Collision-Induced Dissociation. *J. Am. Chem. Soc.* **2003,** *125,* 9229–9236.
12. Schnier, P. D.; Price, W. D.; Jockusch, R. A.; Williams, E. R. Blackbody Infrared Radiative Dissociation of Bradykinin and Its Analogues: Energetics, Dynamics, and Evidence for Salt-Bridge Structures in the Gas Phase. *J. Am. Chem. Soc.* **1996,** *118,* 7178–7189.
13. Price, W. D.; Schnier, P. D.; Jockusch, R. A.; Strittmatter, E. F.; Williams, E. R. Unimolecular Reaction Kinetics in the High-Pressure Limit without Collisions. *J. Am. Chem. Soc.* **1996,** *118,* 10640–10644.
14. Schnier, P. D.; Price, W. D.; Strittmatter, E. F.; Williams, E. R. Dissociation Energetics and Mechanisms of Leucine Enkephalin $(M + H)^+$ and $(2M + X)^+$ ions (X = H, Li, Na, K, and Rb) Measured by Blackbody Infrared Radiative Dissociation. *J. Am. Soc. Mass Spectrom.* **1997,** *8,* 771–780.
15. Nemykin, V. N.; Laskin, J.; Basu, P. Isolation, Characterization of an Intermediate in an Oxygen Atom-Transfer Reaction, and the Determination of the Bond Dissociation Energy. *J. Am. Chem. Soc.* **2004,** *126,* 8604–8605.
16. Laskin, J. Energetics and Dynamics of Fragmentation of Protonated Leucine Enkephalin from Time- and Energy-Resolved Surface-Induced Dissociation Studies. *J. Phys. Chem. A* **2006,** *110,* 8554–8562.
17. Yoon, S. H.; Kim, M. S. Development of a Time-Resolved Method for Photodissociation Mechanistic Study of Protonated Peptides: Use of a Voltage-Floated Cell in a Tandem Time-of-Flight Mass Spectrometer. *J. Am. Soc. Mass Spectrom.* **2007,** *18,* 1729–1739.
18. Yoon, S. H.; Chung, Y. J.; Kim, M. S. Time-Resolved Photodissociation of Singly Protonated Peptides with an Arginine at the N-Terminus: A Statistical Interpretation. *J. Am. Soc. Mass Spectrom.* **2008,** *19,* 645–655.
19. Moon, J. H.; Yoon, S. H.; Kim, M. S. Temperature of Peptide Ions Generated by Matrix-Assisted Laser Desorption Ionization and Their Dissociation Kinetic Parameters. *J. Phys. Chem. B* **2009,** *113,* 2071–2076.
20. Yoon, S. H.; Moon, J. H.; Kim, M. S. Time-Resolved Photodissociation Study of Singly Protonated Peptides with a Histidine Residue Generated by Matrix-Assisted Laser Desorption Ionization: Dissociation Rate Constant and Internal Temperature. *J. Am. Soc. Mass Spectrom.* **2009,** *20,* 1522–1529.
21. Yoon, S. H.; Moon, J. H.; Chung, Y. J.; Kim, M. S. Influence of Basic Residue on Dissociation Kinetics and Dynamics of Singly Protonated Peptides: Time-Resolved Photodissociation Study. *J. Mass Spectrom.* **2009,** *44,* 1532–1537.
22. Holbrook, K. A.; Pilling, M. J.; Robertson, S. H. Unimolecular Reactions; Wiley: Chichester, 1996; p. 39–78.
23. Baer, T.; Mayer, P. M. Statistical Rice-Ramsperger-Kassel-Marcus Quasi-Equilibrium Theory Calculations in Mass Spectrometry. *J. Am. Soc. Mass Spectrom.* **1997,** *8,* 103–115.
24. Moon, J. H.; Yoon, S. H.; Kim, M. S. Construction of an Improved Tandem Time-of-Flight Mass Spectrometer for Photodissociation of Ions Generated by Matrix-Assisted Laser Desorption Ionization (MALDI). *Bull. Korean Chem. Soc.* **2005,** *26,* 763–768.
25. Bae, Y. J.; Yoon, S. H.; Moon, J. H.; Kim, M. S. Optimization of Reflectron for Kinetic and Mechanistic Studies with Multiplexed Multiple Tandem (MS^n) Time-of-Flight Mass Spectrometry. *Bull. Korean Chem. Soc.* **2010,** *31,* 92–99.
26. Moon, J. H.; Oh, J. Y.; Kim, M. S. A Systematic and Efficient Method to Estimate the Vibrational Frequencies of Linear Peptide and Protein Ions with Any Amino Acid Sequence for the Calculation of Rice-Ramsperger-Kassel-Marcus Rate Constant. *J. Am. Soc. Mass Spectrom.* **2006,** *17,* 1749–1757.
27. Moon, J. H.; Sun, M.; Kim, M. S. Efficient and Reliable Calculation of Rice-Ramsperger-Kassel-Marcus Unimolecular Reaction Rate Constants for Biopolymers: Modification of Beyer-Swinehart Algorithm for Degenerate Vibrations. *J. Am. Soc. Mass Spectrom.* **2007,** *18,* 1063–1069.
28. Gabelica, V.; Schulz, E.; Karas, M. Internal Energy Build-Up in Matrix-Assisted Laser Desorption/Ionization. *J. Mass Spectrom.* **2004,** *39,* 579–593.
29. Luo, G.; Marginean, I.; Vertes, A. Internal Energy of Ions Generated by Matrix-Assisted Laser Desorption/Ionization. *Anal. Chem.* **2002,** *74,* 6185–6190.
30. Alexander, A. J.; Boyd, R. K. Experimental Investigations of Factors Controlling the Collision Induced Dissociation Spectra of Peptide Ions in a Tandem Hybrid Mass Spectrometer. I. Leucine Enkephalin. *Int. J. Mass Spectrom. Ion Processes* **1989**, *90,* 211–240.
31. Dunbar, R. C. BIRD (Blackbody Infrared Radiative Dissociation): Evolution, Principles, and Applications. *Mass Spectrom. Rev.* **2004,** *23,* 127–158.
32. Troe, J.; Ushakov, V. G.; Viggiano, A. A. On the Model Dependence of Kinetic Shifts in Unimolecular Reactions: The Dissociation of the Cations of Benzene and n-Butylbenzene. *J. Phys. Chem. A* **2006,** *110,* 1491–1490.
33. Stevens, W.; Sztáray, B.; Shuman, N.; Baer, T.; Troe, J. Specific Rate Constants $k(E)$ of the Dissociation of Halobenzene Ions: Analysis by Statistical Unimolecular Rate Theories. *J. Phys. Chem. A* **2009,** *113,* 573–582.
34. Knochenmuss, R. Ion Formation Mechanisms in UV-MALDI. *Analyst* **2006,** *131,* 966–986.
35. Knochenmuss, R.; Zenobi, R. MALDI Ionization: The Role of In-Plume Processes. *Chem. Rev.* **2003,** *103,* 441–452.
36. Chesnavich, W. J.; Bass, L.; Su, T.; Bowers, M. T. Multiple Transition States in Unimolecular Reactions: A Transition State Switching Model. Application to the $C_4H_8^{+\cdot}$ System. *J. Chem. Phys.* **1981,** *74,* 2228–2245.